Received: 17 March 2020 | Revised: 27 May 2020 | Accepted: 29 May 2020

DOI: 10.1002/aoc.5889

Applied Organometallic Chemistry WILEY

FULL PAPER

Ferrocenylmethylation of estrone and estradiol: Structure, electrochemistry, and antiproliferative activity of new ferrocene–steroid conjugates

Vidak Raičević[1] | Niko Radulović[2] | Ljiljana Jovanović[1] | Marko Rodić[1] | Ivana Kuzminac[1] | Dimitar Jakimov[3] | Tanja Wrodnigg[4] | Tim-Oliver Knedel[5] | Christoph Janiak[5] | Marija Sakač[1]

[1]Department of Chemistry, Biochemistry and Environmental Protection, Faculty of Sciences, University of Novi Sad, Trg Dositeja Obradovića 3, Novi Sad, 21000, Serbia

[2]Department of Chemistry, Faculty of Sciences and Mathematics, University of Niš, Višegradska 33, Niš, 18000, Serbia

[3]Oncology Institute of Vojvodina, Put doktora Goldmana 4, Sremska Kamenica, 21204, Serbia

[4]Glycogroup, Institute of Chemistry and Technology of Biobased Systems, Graz University of Technology, Stremayrgasse 9, Graz, A-8010, Austria

[5]Institute for Inorganic Chemistry and Structural Chemistry, Heinrich-Heine-Universität Düsseldorf, Universitätsstraße 1, Düsseldorf, D-40225, Germany

Correspondence
Vidak Raičević, Marija Sakač, Department of Chemistry, Biochemistry and Environmental Protection, Faculty of Sciences, University of Novi Sad, Trg Dositeja Obradovića 3, 21000 Novi Sad, Serbia.
Email: vidak.raicevic@dh.uns.ac.rs; marija.sakac@dh.uns.ac.rs

Funding information
This work was supported by the Ministry of Education, Science and Technological Development of the Republic of Serbia.

Conjugates of ferrocene with steroidal estrogens as selective antiproliferative agents against hormone-dependent breast cancer cells are believed to be limited by the inherent estrogenicity of the conjugates. Motivated by a significant cytotoxicity of the ester of ferrocenecarboxylic acid and the phenolic group of estradiol toward such a cell line, we decided to explore other A-ring-tethered ferrocene–estra-1,3,5(10)-triene conjugates; in this study, ferrocenylmethylation of estradiol and estrone with (ferrocenylmethyl) trimethylammonium iodide in the presence of potassium carbonate yielded five new compounds (**1**–**5**). In dimethylformamide, only *O*-alkylated products formed (**1** and **3**), while a mixture of *O*- and *C*-alkylated products was obtained when methanol was used (**2**, **4**, and **5** in addition to **1** and **3**). All compounds were characterized using 1D and 2D NMR, IR, UV–Vis, and high-resolution mass spectrometry. Two of the conjugates, a 3-*O*- and a 4-*C*-alkylated derivative of estrone (**3** and **4**, respectively), were also analyzed using single-crystal X-ray diffraction. A cyclic voltammetric investigation of the electrochemical properties of **1**–**5** was performed. While some of the compounds were shown to have a slight-to-moderate antiproliferative activity against at least one of the six tested human tumor cell lines and were nontoxic to (the noncancerous) fetal human fibroblasts, compound **2** (4-(ferrocenylmethyl)estra-1,3,5(10)-triene-3,17β-diol) with an IC_{50} value of 0.34 μM was found to be more active against the hormone-dependent breast cancer cell line MCF-7 than doxorubicin. These results suggest that A-ring substitution of steroidal estrogens is a plausible strategy for preparing other ferrocene–steroid conjugates acting against tumor cells.

KEYWORDS
breast cancer, cyclic voltammetry, estrogens, ferrocene, X-ray crystallography

[Corrections added on 15 July 2020, after first online publication: Typographical mistakes were corrected in the abstract and page running head, and the resolution of Figures 1, 2 and Scheme 1 was improved.]

1 | INTRODUCTION

Breast cancer is the most common cancer among women worldwide and a major cause of mortality,[1] where the prevailing number of cases of breast cancer is hormone-dependent.[2] The proliferation of such tumors is promoted by naturally occurring estrogens, most notably estradiol (E2) and estrone (E1). These compounds activate estrogen receptor alpha (ERα), a protein expressed in all hormone-dependent breast cancer cells.[3] The long-established drug tamoxifen, a selective estrogen receptor modulator, is currently the treatment of choice for this condition.[4,5] However, it is prone to acquired resistance and may cause a variety of serious side effects, including endometrial cancer, blood clotting, and stroke.[6] Consequently, the development of alternative agents has been under way for some time.[5,7]

Although the accidental discovery of ferrocene in 1951 sparked the development of modern organometallic chemistry,[8] it was not until the 1980s that its compounds captured the interest of medicinal chemists as potential anticancer drugs. Particularly important was the discovery that ferrocenium salts inhibited the growth of the Ehrlich ascites tumor,[9] presumably via oxygen radical species that form in Fenton-type reactions when the ferrocenium cation degrades in aqueous media.[10] Subsequently, neutral ferrocene–containing compounds exhibiting cytotoxicity were also synthesized; it was suggested that oxidation of these ferrocene derivatives to the corresponding ferrocenium species in biological systems could be causing the cytotoxic effect.[11–13] This seminal work was published in this very journal[12] almost 30 years ago and put forward the idea that potential advantages of neutral molecules relative to ferrocenium salts include increased stability and bioavailability.[14] Currently many ferrocene derivatives are known to possess antiproliferative properties.[14,15]

With this in mind, it was reasonable to advance a hypothesis that incorporating a ferrocene moiety into the structure of an ERα bioligand could provide the means to transport and concentrate potentially cytotoxic compounds in hormone-dependent breast cancer cells.[16] This was first explored by Jaouen's group; in a series of publications, 17α- or 7α-substituted ferrocene–E2 conjugates were prepared (**I**–**III**, Figure 1), with or without the presence of a linker between ferrocene and the steroid backbone.[17] However, all of these compounds were found to behave as estrogens, inducing *in vitro* proliferation of a hormone-dependent breast cancer cell line (MCF-7), and having high binding affinities for ERα. Several ferrocene–steroid estrogen conjugates, including ferrocenecarboxylic acid esters and 16-(ferrocenylmethylidene) derivatives of E2 (**IV**) or E1 (**V**), were synthesized by Wenzel's group (Figure 1).[18] These studies aimed to prepare radiopharmaceuticals based on Ru-103 and Tc-99m to study organ distribution of estrogens, and the ferrocene–steroid conjugates only served as precursors. The 16-(ferrocenylmethylidene) derivatives of E2 and E1 were also subsequently reported by Manosroi[19] and Mélendez[20]; the latter paper also reported **IV** as being cytotoxic to hormone-dependent breast cancer cell lines MCF-7 and T-47D in medium micromolar IC_{50} range.

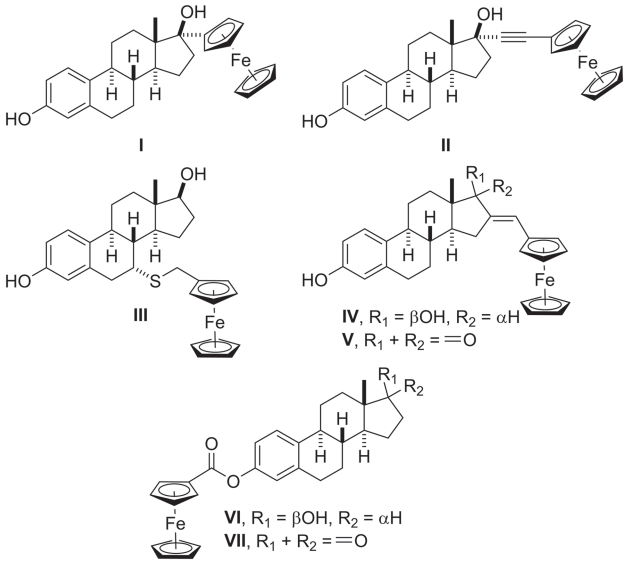

FIGURE 1 Some conjugates of estra-1,3,5(10)-trienes with ferrocene

The affinity of steroidal estrogens toward ERα is known to be strongly affected by A-ring substituents.[21] To date, some estra-1,3,5(10)-trienes bearing a ferrocene-containing group at ring A have been prepared. Apart from a 3,17-disubstituted derivative designed as an amphiphile precursor,[22] these compounds are limited to the previously mentioned hydrolysis-prone ferrocenecarboxylic acid phenolic esters.[23,24] Although one would expect A-ring derivatives to have difficulty binding to the ERα active site, the outcome of such hybridization is not easily predictable. Expectedly, the ester of ferrocenecarboxylic acid and E1 (**VII**, Figure 1) was found to lack substantial cytotoxicity; however, the ester of this acid and the phenol of E2 (**VI**, Figure 1) was significantly more effective in lowering the proliferation of MCF-7 cells.[24] The authors proposed that the onset of cytotoxicity came from a non-active site binding of the E2–ferrocene conjugate.[24] As we believe that the redox chemistry of the ferrocene core also plays an important role in the cytotoxic potential of such estrogen-ferrocene hybrids, an electron-donor tether, a methylene group, as opposed to a carbonyl

would make the metallocene more prone to oxidation to the cytotoxic ferrocenium ion. Prompted by these considerations and as part of our efforts to synthesize steroidal compounds acting as antiproliferative agents and biologically active ferrocene derivatives,[25] we prepared five new ferrocene–steroid conjugates by A-ring ferrocenylmethylation of E2 and E1. Herein we report the synthesis of these conjugates, their spectral characterization, molecular structure by single-crystal X-ray diffraction, as well as electrochemical and antiproliferative properties that revealed that A-ring substitution can be a promising strategy for the future development of antiproliferative agents.

2 | EXPERIMENTAL

2.1 | Materials and methods

(Ferrocenylmethyl)trimethylammonium iodide was prepared according to a published procedure.[26] All other chemicals were used as obtained from commercial suppliers unless stated otherwise. Thin layer chromatography was performed on Merck (Darmstadt, Germany) silica gel 60 plates (layer thickness 0.2 mm) with F_{254} indicator. Plate visualizations were accomplished with UV light, and by color reactions, after spraying with 50% (v/v) aqueous H_2SO_4, followed by brief heating on a hotplate. Flash column chromatography was carried out on neutralized silica gel prepared in a manner similar to that reported by Nagy,[27] except that silica gel 60(0.04–0.063 mm, Merck) was suspended in 0.1 M aqueous NaOH and stirred for 30 min at room temperature. Sephadex LH-20 (Merck) was swollen in a 1:1 (v/v) mixture of chloroform and methanol. Melting points were determined on a Büchi Melting Point B-540 apparatus (Büchi Labortechnik AG, Flawil, Switzerland) and were uncorrected. IR measurements were carried out on thin films deposited on a KBr plate from solutions of compounds **1**, **3**, **4**, and **5** in CH_2Cl_2 on a Spectrum Two spectrometer (PerkinElmer, Waltham, MA, USA), or as a KBr pellet on a Thermo Nicolet NEXUS 670 FTIR spectrometer (Thermo Scientific, Waltham, MA, USA) for compound **2**. The UV–Vis. spectra were recorded in acetonitrile on a T80 + UV/Vis Spectrophotometer (PG Instruments, Ltd., Lutterworth, UK). ^1H and $^{13}C\{^1H\}$ NMR spectra were recorded on a Bruker Avance III spectrometer (Bruker, Rheinstetten, Germany) equipped with a CryoProbe Prodigy probe-head, operating at 400 and 100.6 MHz, respectively. 2D experiments (gradient ^1H–^1H COSY, HSQC, and HMBC, and NOESY) were run on the same instrument utilizing the built-in Bruker pulse sequences. All NMR spectra were measured at 25 °C in deuterated chloroform with either tetramethylsilane or residual $CHCl_3$ (δ_H 7.26) and $^{13}CDCl_3$ (δ_C 77.16) as the internal reference standards. Matrix-assisted laser desorption/ionization-time of flight mass spectrometry was performed on a Micromass TofSpec 2E Time-of-Flight mass spectrometer (Waters Corporation, Milford, MA, USA). Spectra and additional supporting information may be found online in the Supporting Information section at the end of this article.

2.2 | Synthesis and characterization of ferrocene–steroid conjugates 1–5

2.2.1 | Ferrocenylmethylation in DMF

A suspension of K_2CO_3 (152 mg, 1.10 mmol), E1 or E2 (0.55 mmol), and (ferrocenylmethyl)trimethylammonium iodide (425 mg, 1.10 mmol) was heated at 100 °C for 12 h in DMF (10 ml) under an atmosphere of argon. The mixture was cooled to room temperature, diluted with brine, and extensively extracted with diethyl ether (5 × 25 ml). The pooled ether solution was then washed with brine (5 × 30 ml), dried over anhydrous sodium sulfate, and evaporated to dryness. The crude product was subjected to flash column chromatography on neutralized silica gel (eluent: benzene for E1, benzene/ethyl acetate 25:1, v/v, for E2).

2.2.2 | Ferrocenylmethylation in MeOH

A suspension of K_2CO_3 (152 mg, 1.10 mmol), E1 or E2 (0.55 mmol), and (ferrocenylmethyl)trimethylammonium iodide (425 mg, 1.10 mmol) in methanol (10 mL) was refluxed for 20 h under an atmosphere of argon. The mixture was concentrated in vacuo and cooled to room temperature, and the suspension was extracted with diethyl ether (25 ml). After filtration, the resulting solid was washed with a small amount of diethyl ether. The combined ethereal solution was then washed with brine (3 × 10 ml), dried over anhydrous sodium sulfate, and evaporated to dryness. The product mixture was separated by flash column chromatography on neutralized silica gel (eluent: benzene for E1, benzene/ethyl acetate 25:1, v/v, for E2).

2.2.3 | 3-(Ferrocenylmethoxy)estra-1,3,5(10)-trien-17β-ol (1)

Yield: 63% in DMF, 32% in MeOH; orange solid; m. p. 144 °C (from chloroform, decomposes); IR (CH_2Cl_2 film) ν_{max} cm^{-1}: 3401 (O–H), 2923, 2868, 1607,

1498, 1249, 1053; UV–Vis. (MeCN) λ_{max} nm (log ε): 236 (3.74), 278*sh* (3.46), 286*sh* (3.34), 323 (2.00), 437 (2.05) (*sh*, shoulder); ^{1}H NMR: see Table 2; ^{13}C NMR: see Table 3; HRMS: Calcd. for $C_{29}H_{34}FeO_2$: 470.1908, found: 470.1909.

2.2.4 | 4-(Ferrocenylmethyl)estra-1,3,5(10)-triene-3,17β-diol (2)

Yield: 0% in DMF, 9% in MeOH; orange solid; m. p. 138 °C (from chloroform, decomposes); IR (KBr) ν_{max} cm^{-1}: 3434 (O–H), 2924, 2867, 1635, 1446, 1279, 1058; UV–Vis. (MeCN) λ_{max} nm (log ε): 233 (3.84), 278*sh* (3.58), 286*sh* (3.51), 323 (2.37), 438 (2.16); ^{1}H NMR: see Table 2; ^{13}C NMR: see Table 3; HRMS: Calcd. for $C_{29}H_{34}FeO_2$: 470.1908, found: 470.1910.

2.2.5 | 3-(Ferrocenylmethoxy)estra-1,3,5(10)-trien-17-one (3)

Yield: 66% in DMF, 33% in MeOH; orange solid; m. p. 155 °C (from chloroform, decomposes); IR (CH_2Cl_2 film) ν_{max} cm^{-1}: 2927, 2862, 1738 (C=O), 1608, 1499, 1247, 1053; UV–Vis. (MeCN) λ_{max} nm (log ε): 237 (3.81), 277*sh* (3.50), 285*sh* (3.36), 316 (2.22), 435 (2.09); ^{1}H NMR: see Table 2; ^{13}C NMR: see Table 3; HRMS: Calcd. for $C_{29}H_{32}FeO_2$: 468.1752, found: 468.1752.

2.2.6 | 4-(Ferrocenylmethyl)-3-hydroxyestra-1,3,5(10)-trien-17-one (4) and 2-(ferrocenylmethyl)-3-hydroxyestra-1,3,5(10)-trien-17-one (5)

A mixture of **4** and **5** in 7:3 ratio; total yield: 0% in DMF, 10% in MeOH; orange solid; IR (CH_2Cl_2 film) ν_{max} cm^{-1}: 3401 (O–H), 2927, 1723 (C=O), 1610, 1452, 1280, 1033; UV–Vis. (MeCN) λ_{max} nm (log ε): 231 (3.78), 279*sh* (3.51), 325*sh* (2.25), 439 (2.06); ^{1}H NMR: see Table 2; ^{13}C NMR: see Table 3; HRMS: Calcd. for $C_{29}H_{32}FeO_2$: 468.1752, found: 468.1755.

2.3 | X-ray crystallography

The single-crystal X-ray diffraction data were collected using a Bruker Kappa APEX II diffractometer (for compound **3**) and an Oxford Diffraction Gemini S diffractometer (for compound **4**). Diffraction data for compounds **3** and **4** were processed using Bruker APEX 3 (APEX 3, Bruker AXS Inc., 2016, Madison, WI, USA) and CrysAlis^{Pro} software (CrysAlis^{Pro} Software System, Rigaku Oxford Diffraction, 2015, Rigaku Corporation, Oxford, UK), respectively. The structures were solved using SHELXT,[28] refined by SHELXL-2018[29] using SHELXLE[30] as a graphical user interface. The structure of **4** showed positional disorder in the non-substituted cyclopentadienyl ring. A highly constrained disorder model was preferred over a "static" model with elongated anisotropic displacement parameters (ADPs) based on the evaluation of $R_{complete}$ values[31] for both models. Absolute structures have been assigned by both references to several unchanging chiral centers in the synthetic procedure, and by anomalous-dispersion effects in diffraction measurements on the crystals. PLATON[32] and Mercury CSD[33] were used to validate and analyze the crystal structures. Crystallographic data associated with this publication are deposited with the Cambridge Crystallographic Data Centre under the CCDC Numbers 1,989,147–1,989,148. They are available for free at https://www.ccdc.cam.ac.uk/structures. Crystallographic and refinement details are listed in Table 1. Hirshfeld surface analysis[34] was performed with Crystal Explorer.[35] Intermolecular interaction energies, calculated for all intermolecular pairs surrounding the Hirshfeld surface of the central molecule using CE-B3LYP model energies,[36] were used to construct energy frameworks.[37]

2.4 | Cyclic voltammetry

Cyclic voltammetry experiments were performed at room temperature on a VoltaLab PST050 (Radiometer Analytical, Lyon, France) with a glassy carbon-disk (GC) working electrode (3 mm in diameter), a platinum wire counter electrode, and a reference saturated calomel electrode (SCE). All potentials are reported against this electrode. The measurements were carried out in analytical-grade DMF, which was doubly distilled after being dried according to a published procedure.[38] The supporting electrolyte was 0.1 M tetrabutylammonium perchlorate recrystallized prior to solution preparation. The experiments were carried out under an inert atmosphere of nitrogen.

2.5 | Cell lines and cell culture

Seven human cell lines were used in this study: estrogen receptor-positive breast adenocarcinoma MCF-7 (American Type Culture Collection, ATCC HTB22), estrogen receptor-negative breast adenocarcinoma MDA-MB-231 (ATCC HTB26), prostate cancer PC-3

TABLE 1 Crystallographic and refinement details of **3** and **4**

	3	**4**
Chemical formula	$C_{29}H_{32}FeO_2$	$C_{29}H_{32}FeO_2$
M_r	468.39	468.39
Crystal system	Orthorhombic	Orthorhombic
Space group	$P2_12_12_1$	$P2_12_12_1$
Temperature (K)	140	293
a (Å)	6.7898 (10)	7.4416 (3)
b (Å)	12.1966 (18)	13.1083 (7)
c (Å)	27.257 (4)	23.9139 (13)
V (Å^3)	2257.3 (6)	2332.7 (2)
Z	4	4
Radiation type	Mo $K\alpha$	Mo $K\alpha$
μ (mm^{-1})	0.69	0.67
Crystal size (mm)	0.10 × 0.05 × 0.02	0.37 × 0.20 × 0.12
Diffractometer	Bruker Kappa APEX II	Oxford Diffraction Gemini S
Absorption correction	Multiscan	Analytical
T_{min}, T_{max}	0.816, 1.000	0.820, 0.929
Measured reflections	16,708	16,258
Independent reflections	5150	5381
Observed reflections [$I > 2\sigma(I)$]	3581	4394
R_{int}	0.132	0.049
$(\sin\theta/\lambda)_{max}$ (Å^{-1})	0.649	0.682
$R[F^2 > 2\sigma(F^2)]$	0.053	0.099
$wR(F^2)$	0.114	0.268
S	0.92	1.10
No. of reflections	5150	5381
No. of parameters	290	338
No. of restraints	0	179
H-atom treatment	Constrained	Constrained
$\Delta\rho_{max}$, $\Delta\rho_{min}$ (e Å^{-3})	0.43, −0.30	1.16, −0.83
Absolute structure	Flack x determined using 1070 quotients	Refined as an inversion twin
Flack x	−0.03 (2)	0.10 (7)

(ATCC CRL-1435), cervical carcinoma HeLa (ATCC CCL-2), colon adenocarcinoma HT-29 (ATCC HTB-38), lung adenocarcinoma A549 (ATCC CCL-185), and normal fetal lung fibroblasts MRC-5 (ATCC CCL-171). Cells were grown in Dulbecco's modified Eagle medium (DMEM) containing 0.45% (w/v) glucose, supplemented with 10% fetal calf serum (Sigma Aldrich, St. Louis, MO, USA) and an antibiotics/antimycotic solution (Sigma Aldrich). Cells were cultured in flasks (size 25 cm^2, Costar, Sigma Aldrich) at 37 °C in 100% humidity with 5% (v/v) CO_2. Cell viability was determined by trypan blue exclusion assay.

2.6 | Antiproliferative activity assay

Compounds **1–5** were evaluated for antiproliferative activity using the tetrazolium colorimetric MTT assay.[39] Cells were exposed to test compounds for 72 h in concentrations ranging from 10^{-8} to 10^{-4} M. Doxorubicin (DOX) is a nonselective antiproliferative agent used as a general cytotoxicity control. Exponentially growing cells were harvested, counted by trypan blue exclusion, and plated onto 96-well microtiter plates (Costar, Sigma Aldrich) at an optimal seeding density of 5000 cells per well to assure a logarithmic growth rate throughout the assay period. Viable cells were plated in a volume of 90 µl per well and pre-incubated in the complete medium at 37 °C for 24 h to ensure cell stabilization before the addition of test compounds. All of the test compounds were dissolved in DMSO and diluted with the growth medium to obtain solutions possessing 10 times higher concentrations than the required final concentrations. Such solutions (10 µl per well) were added to all wells, and the microplates were incubated for 24 h. Wells containing cells without the tested compounds were used as a reference. MTT was dissolved in the medium at 5 mg ml^{-1} and filter sterilized to remove a small amount of insoluble residue present in some batches of MTT. Three hours before the end of the incubation period, 10 µl of MTT solution was added to each well. Acidified isopropanol (100 µl of 0.04 M HCl in aqueous isopropanol) was added to each well and mixed thoroughly to dissolve the dark-blue crystals. After a few minutes of incubation at room temperature (to ensure that all MTT dissolved), plates were read on a spectrophotometric plate reader (Multiskan MCC340, Labsystems, Thermo Scientific, Waltham, MA, USA) at 540 nm with background correction at 690 nm. Wells without any cells, containing the complete medium and MTT only, were used as the blank. Mean values and standard deviations were calculated for each concentration. Two independent experiments were conducted in quadruplicate for each concentration of the

tested compound. The antiproliferative activity was expressed as IC_{50} (50% inhibitory concentration), determined by median effect analysis.

2.7 | Statistical analysis

In antiproliferative tests, statistically significant differences were determined by one-way analysis of variance (ANOVA) followed by Tukey's post-hoc test for multiple comparisons (GraphPad, Prism version 5.03, San Diego, CA, USA). Probability values (P) ≤ 0.05 were considered to be statistically significant.

3 | RESULTS AND DISCUSSION

3.1 | Synthesis

We chose (ferrocenylmethyl)trimethylammonium iodide (**VIII**, Scheme 1) as the reagent for ferrocenylmethylation of E2 and E1; this salt was reported to react with various nucleophiles, effecting alkylation by the loss of trimethylamine.[40] It was suspected that the steroid phenolate would likewise yield a ferrocenylmethyl ether-type conjugate. The reactions with the two steroidal estrogens were assayed in two different solvents, one aprotic (*N*,*N*-dimethylformamide) and one protic (methanol), in both cases in the presence of potassium carbonate as the base. The reaction outcomes are summarized in Scheme 1.

The reactions of E2 and E1 in DMF with the methiodide **VIII** expectedly yielded exclusively products of *O*-ferrocenylmethylation, producing ethers **1** and **3** in moderate yields (63% and 66%, respectively). Though in more modest yields (32% and 33%, respectively), these two compounds were also isolated from the product mixtures obtained when the reactions were conducted in methanol. However, in addition to the ether products, the reactions in methanol resulted in the formation of *C*-ferrocenylmethylation products. While 4-(ferrocenylmethyl) derivative **2** was the sole *C*-alkylation product obtained in a 9% yield from E2, a 7:3 mixture of 4- and 2-(ferrocenylmethyl) derivatives **4** and **5** was obtained starting from E1 in a similar total yield (10%). This regioisomeric mixture proved inseparable by preparative column chromatography on normal-phase silica gel. In the case of chromatography on Sephadex LH-20, some separation was observed (Figure S9), but insufficient pure material was obtained after successive separations to allow additional chemical characterization and biological tests of pure **4** and **5**; therefore, the data of **4** and **5** were either inferred from mixtures or relate to the mixture of the two isomers.

It is known that α-metallocenyl carbocations are thermally stable species; while it remains to be definitively proved, indirect experimental data offer support for an S_N1 mechanism of alkylation with **VIII.**[40] While *O*-ferrocenylmethylation of phenols (phenol itself and 2-naphthol) with **VIII** was previously reported,[41] *C*-alkylated products have not yet been observed as products of this reaction. It is known, however, that in protic solvents the nucleophilicity of the phenoxide oxygen is decreased as a consequence of hydrogen bonding, which in turn promotes *C*-alkylation. This could account for the formation of products **2**, **4**, and **5** when the ferrocenylmethylation is carried out in methanol. Product yields indicate that in this case *C*-alkylation preferentially occurs at position 4 of the steroid core. An alternative explanation would involve a single-electron transfer reaction that would become faster than the conventional S_N1 due to the aforementioned hydrogen bonding, that is, the electron transfer between the electron-rich phenoxide and the ferrocenylmethyl cation would yield two stable radicals. The inherent *C*-reactivity is more pronounced in the case of the phenoxide radical compared to the anion, leading to *C*-alkylation. To probe this mechanistic assumption,

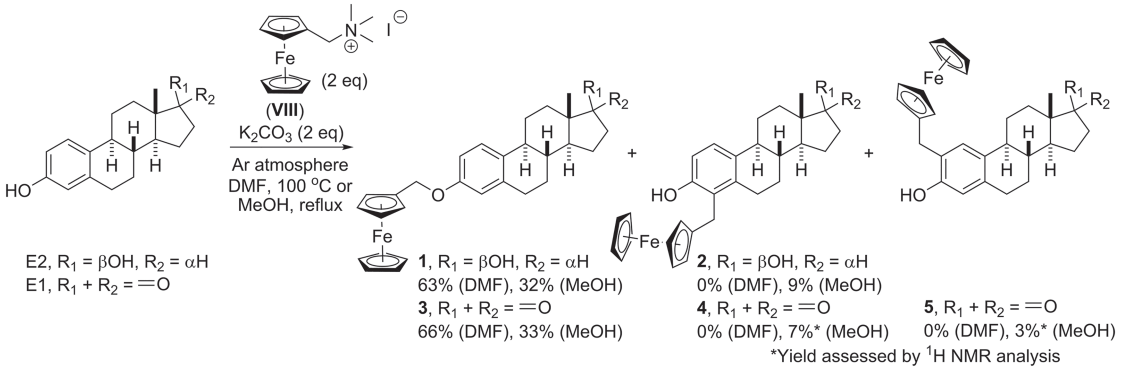

SCHEME 1 Ferrocenylmethylation of E2 and E1

when the reaction was conducted in the absence of the protective atmosphere, oxygen most probably impeded the radical mechanism, lowering the yields of *C*-alkylated products (less than 5%). At this point, we believe that the two mechanisms are both viable and that reaction conditions dictate which of the two prevails.

3.2 | Spectral characterization

The structures of compounds **1**–**5** were confirmed using high-resolution mass spectrometry (HRMS), IR, UV–Vis., 1D (^{1}H and ^{13}C{^{1}H}) and 2D (NOESY, and gradient ^{1}H–^{1}H COSY, multiplicity-edited HSQC, and HMBC) NMR spectroscopy. The molecular formulas of the synthesized compounds were confirmed by the results of high-resolution mass spectrometric measurements (Δ for **1**–**5** + 0.1, +0.2, 0, +0.3 mmu, respectively). The presence or absence of hydroxyl groups (∼3400 cm^{-1}) was routinely inferred from IR. The UV–Vis. spectra of compounds **1**–**5** were quite mutually similar, and each contained a very broad, weak band at ∼440 nm arising from two unresolved electron transitions in ferrocene, $^1A_{1g} \rightarrow a^1E_{1g}$ and $^1A_{1g} \rightarrow {}^1E_{2g}$.[42] This absorption band is the cause of the ferrocene-like orange color of the compounds. A weak but narrower band from the $^1A_{1g} \rightarrow b^1E_{1g}$ transition was found at ∼320 nm. There were two maxima in the 210–300 nm range, one at 280 nm corresponding to π → π* transitions of the estra-1,3,5(10)-triene aromatic A ring, and another maximum at ∼230 nm, possibly resulting from a superposition of ferrocene and A-ring end absorptions.

The complete ^{1}H and ^{13}C NMR spectral assignments for compounds **1**–**5** are presented in Tables 2 and 3. The general numbering scheme is illustrated for compound **1** in Figure 2. The ^{1}H NMR spectra of all compounds consisted of three main regions: the A-ring protons resonated at 6.5–7.25 ppm, ferrocene protons at 4.0–5.0 ppm, protons bound to sp^3-carbons of the steroid skeleton at 0.5–3.0 ppm. The key HMBC and NOESY correlations supporting the A-ring substitution patterns of the structures are shown in Figure 3.

The ^{1}H NMR spectra of compounds **1** and **3** contained a spin system of three signals characteristic of a 1,3,4-trisubstituted aromatic core: an *ortho*-coupled doublet (8.5 Hz, H-1), a *meta*-coupled doublet (2.6 Hz, H-4), and the corresponding doublet of doublets (H-2). Accordingly, compounds **2** and **4** possessed only two *ortho*-coupled doublets in the aromatic region of their ^{1}H NMR spectra. The downfield signal corresponding to H-1 exhibited an nOe interaction with a proton later assigned to H-11α; the upfield proton was assigned to H-2. The ^{1}H NMR spectrum of compound **5** displayed two singlets in this region, and these were assigned in a similar manner.

The pattern of signals corresponding to the magnetically inequivalent protons of the monosubstituted ferrocene ring was identical in all five compounds; H-3′ and H-6′ were isochronous, as were H-4′ and H-5′, owing to the remoteness of the chiral centers at C-8 and C-9. In addition, in the ^{1}H NMR spectra of compounds **1** and **3**, the signals of H-4′ and H-5′ overlapped with H-1″–5″. The diastereotopic methylene hydrogens of C-1′ were accidentally isochronous in all compounds except compound **4**, where they appear as an AB quartet.

As with many other steroid molecules, a region of significant signal overlap at 1.0–2.5 ppm in the ^{1}H NMR spectrum hinders multiplet analysis and assignment. This difficulty can be overcome by relying on correlations of the resolved ^{1}H signals (e.g., the protons of ring A and the angular methyl group) with ^{13}C NMR signals. There is usually no significant overlap in the ^{13}C NMR spectra of steroids, and the chemical shift of the overlapped hydrogen signals can be inferred from known carbon signals by the analysis of HSQC spectra. The orientation of diastereotopic hydrogens of the steroid skeleton can be discerned by multiplet analysis and/or NOESY. Using this algorithm, the signals of the steroid skeleton of compounds **1**–**5** were assigned; the chemical shifts were in good agreement with previously published assignments of estra-1,3,5(10)-triene resonances.[43]

3.3 | X-ray crystallography

Compound **3** readily crystallized from chloroform by slow evaporation of the solvent, forming suitable single crystals. Although attempts to resolve the mixture of **4** and **5** by recrystallization from chloroform failed, they produced a minute quantity of single crystals that proved to be those of compound **4**. The molecular structures of compounds **3** and **4** are depicted in Figure 4. All structural parameters of both molecules fall within the expected range found by comparison with libraries of chemically similar fragments using Mogul.[44]

Insight into the structure of the steroid backbone of compounds **3** and **4** was acquired by determining the parameters of ring pucker,[45] which are given in Table S1. The direction of calculation is clockwise in all cases, starting from the lowest-numbered carbon of the steroid skeleton, as per rules of preference given by Boeyens.[46] Ring A is essentially planar in both structures, so the puckering analysis of it was not performed. The puckering parameters of ring B in compound **3** indicate that its conformation is closest to a 7α,8β-half-chair ($^4H_5$), while in compound **4**, this ring approximately

TABLE 2 ^{1}H chemical shifts (ppm) of compounds **1**–**5** in $CDCl_3$; coupling constants in Hertz given in parentheses

Position	1	2	3	4	5
1	7.21 d (8.6)	7.05 d (8.4)	7.21 d (8.5)	7.03 d (8.4)	6.95 s
2	6.75 dd (8.6, 2.6)	6.63 d (8.4)	6.77 dd (8.5, 2.6)	6.61 d (8.4)	–
3–OH	–	4.92 m	–	4.99 s	4.90 s
4	6.68 d (2.6)	–	6.70 d (2.6)	–	6.48 s
6α	2.81–2.93	2.92 dd (17.1, 5.0)	2.88–2.93	2.98 dd (17.1, 5.5)	2.79–2.85[l]
6β		2.74 ddd (17.1, 11.4, 6.7)		2.78[l]	
7α	1.32[c]	1.29[g]	1.48[j]	1.40[n]	1.40[n]
7β	1.88 dddd (12.6, 5.7, 2.6, 2.6)	1.93[f]	2.04[i]	2.06[m]	1.98[m]
8	1.44[c]	1.37[g]	1.61[j]	1.49[n]	1.55[n]
9	2.19[b]	2.17[e]	2.27 ddd (10.6, 10.6, 4.1)	2.23[m]	2.23[m]
11α	2.32 dddd (13.1, 3.7, 3.7, 3.3)	2.28 dddd (13.2, 3.8, 3.8, 3.4)	2.42 dddd (11.9, 3.7, 3.7, 3.1)	2.35[m]	2.35[m]
11β	1.48[c]	1.46[g]	1.53[j]	1.44[n]	1.44[n]
12α	1.28[c]	1.27[g]	1.52[j]	1.49[n]	1.49[n]
12β	1.95 ddd (12.6, 3.3, 3.3)	1.93[f]	1.98[i]	2.00[m]	2.00[m]
14	1.18[c]	1.15[g]	1.56[j]	1.50[n]	1.50[n]
15α	1.70 dddd (12.4, 9.8, 6.9, 3.0)	1.70 dddd (12.4, 10.0, 7.3, 3.1)	2.09[i]	2.04[m]	2.04[m]
15β	1.37[c]	1.35[g]	1.65[j]	1.61[n]	1.61[n]
16α	2.11[b]	2.12[e]	2.16[i]	2.13[m]	2.13[m]
16β	1.48[c]	1.48[g]	2.51 dd (18.8, 8.5)	2.50 dd (18.8, 8.6)	2.50 dd (18.8, 8.6)
17	3.74 m	3.73[d]	–	–	–
18	0.78 s	0.76 s	0.91 s	0.89 s	0.89 s
1′	4.75 s	3.72 s[d]	4.75 s	3.71 d (15.5) 3.76 d (15.5)	3.66 s
3′, 6′	4.31 m	4.20 m	4.32 m	4.32 m	4.22[k]
4′, 5′	4.19[a]	4.03 m	4.19[h]	4.13 m	4.15 m
1″–5′	4.19 s[a]	4.15 s	4.19 s[h]	4.25 s	4.22 s[k]

Note. Superscripts [a–n] refer to groups of overlapped signals.

adopts an 8β-envelope (^{4}E) conformation, but also with a significant half-chair character. This difference might be a consequence of the sterically demanding ferrocenylmethyl group position. Ring C has a nearly perfect 8β,12α-chair conformation ($^{1}C_4$) in both molecules. Similarly, the five-membered ring D was shown to be in a 14α-envelope conformation (E_5).

To understand the intermolecular interactions present in the crystal structures of **3** and **4**, their respective Hirshfeld surfaces were computed (Figure S14) and decomposed into fingerprint plots (Figure 5). Characteristic "wings" can be recognized on the fingerprint plot of **3**, corresponding to C–H···π interactions, realized by C2A–H2A and the planar steroid A ring of a neighboring molecule. The appearance of the "wings" in the fingerprint plot is reminiscent of an element present in the benzene crystal structure fingerprint plot,[34] as here a hydrogen atom is pointing toward the center of the steroid A ring. The calculation of the enrichment ratios (Table S2)[47] of intermolecular contacts reveals that C···H and O···H contacts are enriched ($E_{CH} = E_{OH} = 1.18$), H···H contacts are slightly disfavored ($E_{HH} = 0.97$), and C···O and O···O contacts are completely avoided in the crystal structure ($E_{CO} = E_{OO} = 0$).

The inspection of the fingerprint plot corresponding to **4** reveals spikes characteristic of hydrogen bonds. They correspond to O3–H3···O17^{i} hydrogen bond (O3–H3 = 0.82 Å, H3···O17^{i} = 2.21 Å, O3···O17^{i} = 2.862(11) Å,

TABLE 3 ^{13}C chemical shifts (ppm) of compounds **1**–**5** in $CDCl_3$

Position	1	2	3	4	5
1	126.29	124.16	126.33	124.16	127.21
2	112.23	112.92	112.35	113.02	131.91
3	156.83	151.59	156.99	151.69	151.41
4	114.64	133.08	114.76	132.47	115.56
5	137.95	136.02	137.74	135.81	135.80
6	29.82	27.12	29.71	26.97	29.07
7	27.27	27.39	26.61	26.69	26.55
8	38.86	37.99	38.41	37.53	38.39
9	43.98	44.32	44.03	44.34	43.97
10	132.72	125.76	132.13	125.86	125.00
11	26.32	26.54	25.96	26.14	25.97
12	36.72	36.73	31.63	31.59	31.59
13	43.27	43.16	48.05	47.94	48.03
14	50.05	50.09	50.44	50.46	50.40
15	23.13	23.10	21.63	21.57	21.57
16	30.62	30.64	35.92	35.92	35.89
17	81.94	81.94	220.99	221.09	221.09
18	11.06	11.03	13.90	13.83	13.87
1′	66.48	25.58	66.52	25.58	30.45
2′	82.98	87.42	82.91	87.89	87.53
3′, 6′	69.11	68.80	69.13	69.10	68.83
4′, 5′	68.57	67.19/67.08	68.60	67.45/67.31	67.89/67.84
1″–5′	68.62	68.87	68.64	69.22	69.05

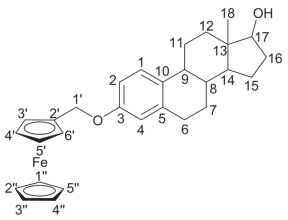

FIGURE 2 The numbering scheme used for NMR assignment (stereochemistry omitted for clarity)

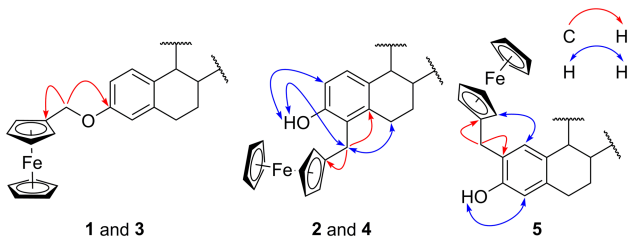

FIGURE 3 Selected HMBC (in red) and NOESY correlations (in blue) of compounds **1**–**5**

O3–H3···O17^{i} = 136.9° (symmetry operation (i) x, $y + 1$, z), which connects the molecules into chains running parallel to the crystallographic axis b. Enrichment ratios reveal an enrichment of C···H and O···H contacts ($E_{CH} = 1.11$, $E_{OH} = 1.12$, Table S2), only a slight disfavoring of H···H contacts ($E_{HH} = 0.98$), while C···O and O···O contacts are actually avoided in the crystal structure ($E_{CO} = 0.43$, $E_{OO} = 0$).

To better understand what determines the crystal packing, a qualitative ranking of specific intermolecular interactions is necessary, as relying solely on geometric parameters can sometimes lead to overlooking stronger and more important interactions.[48] Therefore, we applied the "whole-of-molecule approach" for crystal structures of **3** and **4**, calculating the pairwise intermolecular energies using CE-B3LYP model energies.

The results of the calculations point to a single dominant interaction in the crystal structure of **3**. Namely, the interaction between the closely packed molecules equivalent by translation (symmetry operation $x + 1$, y, z) is dispersion-dominated and stabilizing by −76 kJ mol^{-1}.

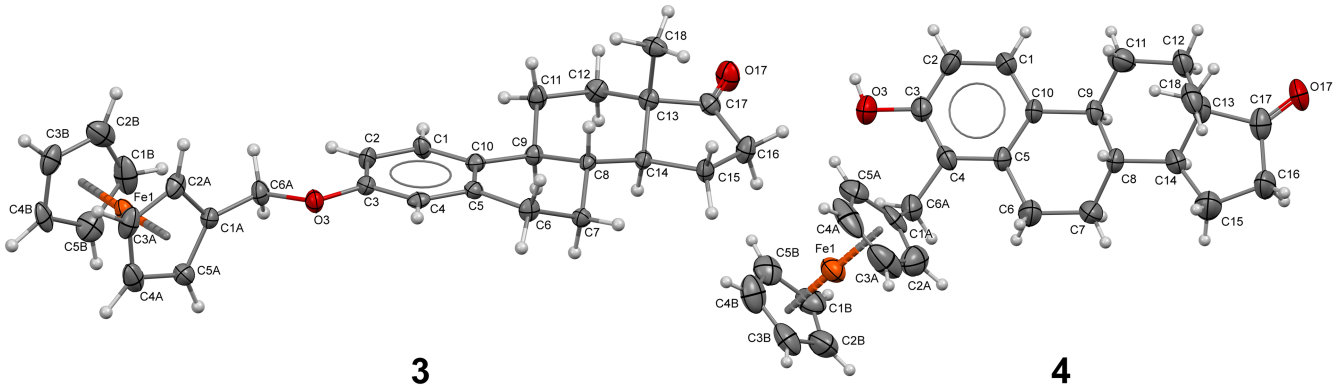

FIGURE 4 Molecular structures of **3** and **4** with atom labeling schemes

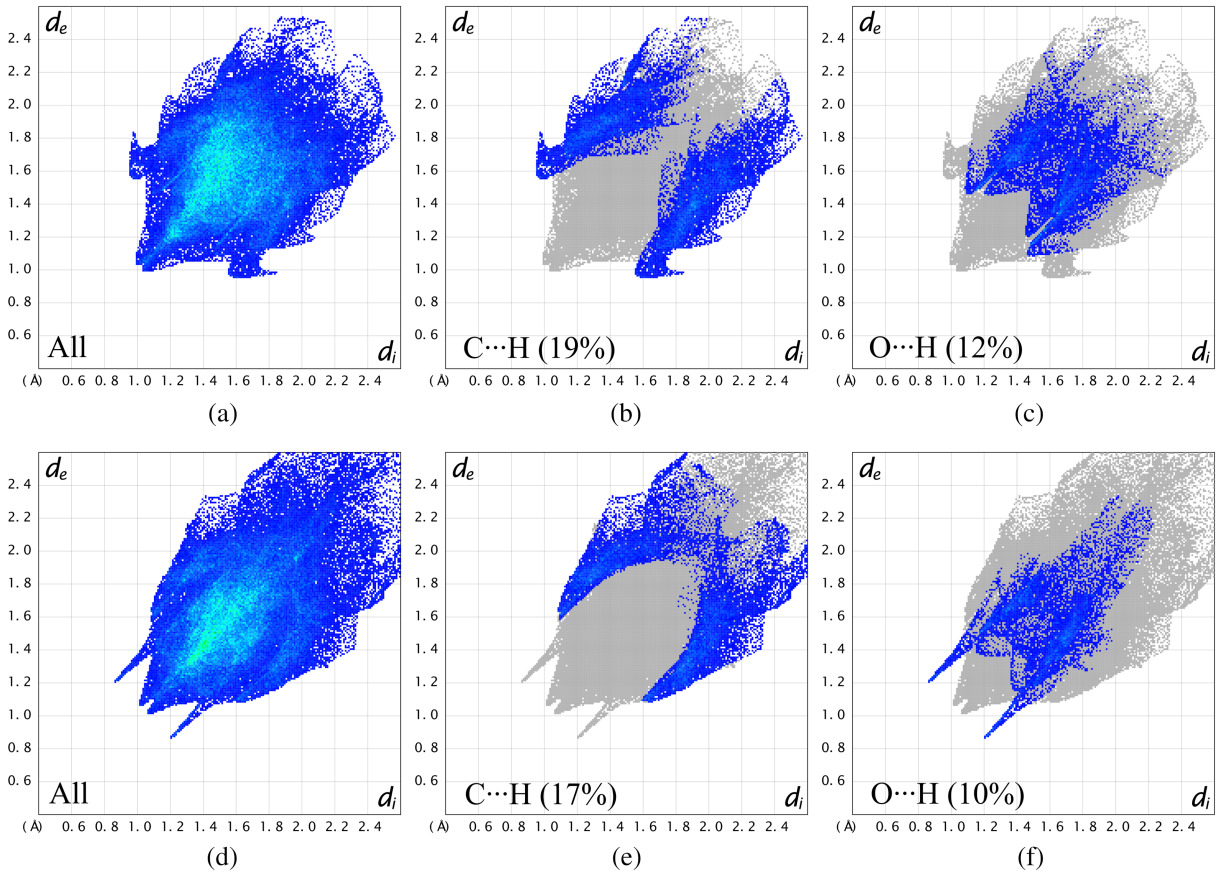

FIGURE 5 Fingerprint plots of **3** (a–c) and **4** (d–f) crystal structures

This interaction stacks molecules into infinite chains running along the crystallographic *a*-axis, which is the basic structural unit of the crystal structure. Also, it is this interaction in which the already-mentioned short C–H···π contacts are observed (Figure S15). Apart from this interaction, there are several other significantly weaker interactions, the energies of which range from −11 to −25 kJ mol^{-1}. All of these are also dominated by dispersion (a total of 18 molecules surround the central one based on Hirshfeld surface analysis). The energetic architecture of the crystal structure of **3** is displayed in Figure 6 through the respective energy framework (a and b). Intermolecular interactions present in the crystal structure of **3** are summarized in Table 4.

The analysis of molecular packing in the crystal structure of **3** indicates the presence of ferrocene–ferrocene dimers,[49] depicted in Figure 7. The central molecule participates in the formation of four such dimers. Molecules I and II are related to the central molecule by translations, and their intermolecular interaction energies are

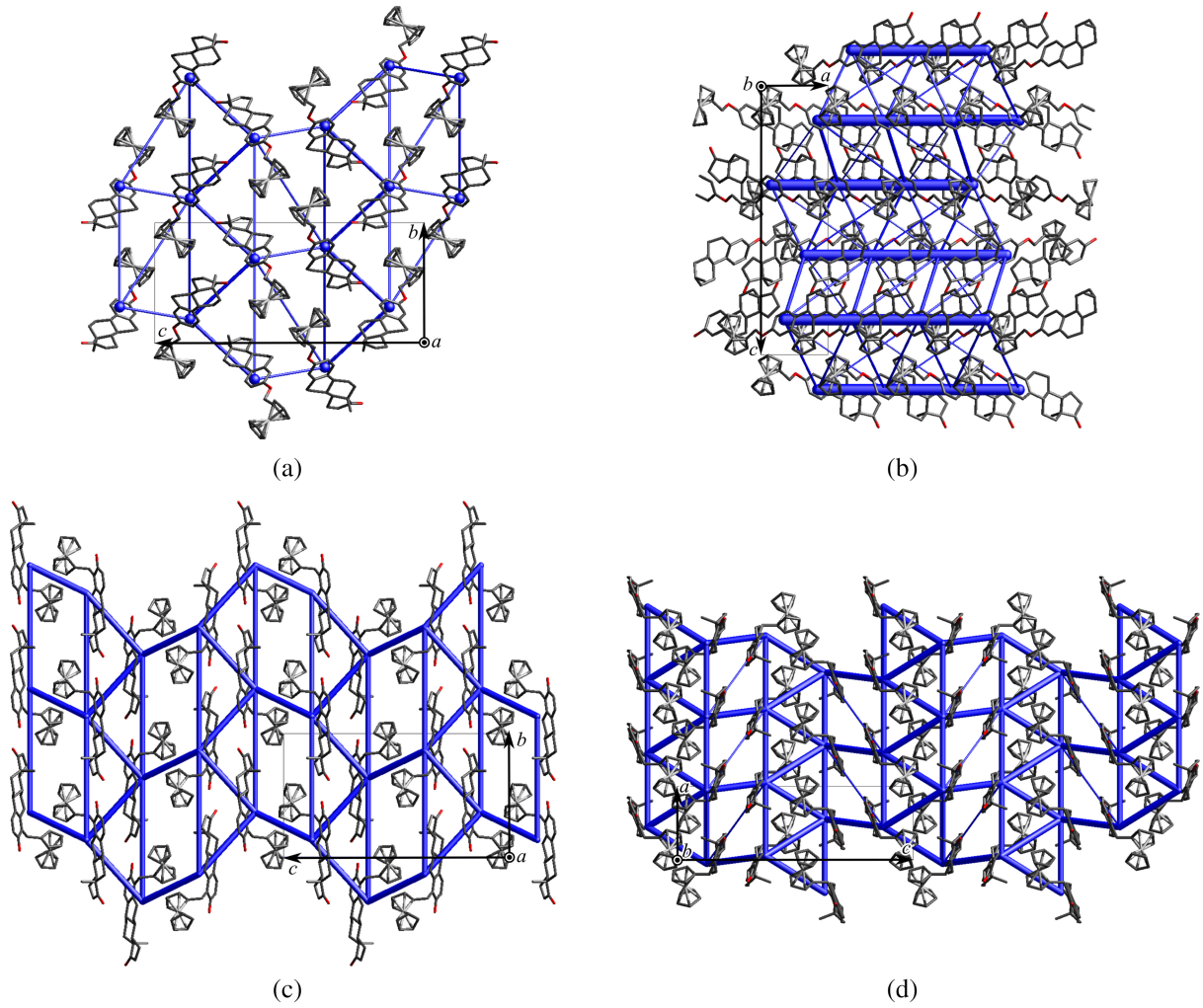

FIGURE 6 Energy frameworks of **3** (a, b) and **4** (c, d)

equal in magnitude. These interactions correspond to the strongest in the crystal structure as already discussed (labeled as 1 in Table 4), but the electrostatic complementarity of ferrocene fragments is not likely to be the major factor contributing to this stabilizing interaction. Namely, apart from the ferrocene moieties, steroid backbones constitute a significant part of the contact surface. As already mentioned, this interaction is dominated by the dispersion term, while its electrostatic term is still the largest among all pairwise interactions of the first coordination shell, due to relatively good pairing of the electrostatic potential on the bordering Hirshfeld surface patches (Figure S16). However, matching is best (largest contact surface area and the absolute value of molecular electrostatic potential [MEP]) between positive MEP patches lateral to the ferrocene moiety and negative MEP patches on the α-side of the ring A of the neighboring molecule.

Dimers formed with molecules III and IV are related to the central molecule by 2_1 screw rotations, and their intermolecular interaction energies are also equal in magnitude. Contrary to the situation for dimers with molecules I and II, here the contacts between neighboring Hirshfeld surfaces are achieved only by patches in the vicinity of ferrocene moieties. However, energy considerations reveal that this interaction is relatively weak (−15 kJ mol^{-1}) and clearly dominated by dispersion, meaning that the matching between MEP on the Hirshfeld surfaces in contact is not significant.

The calculation of intermolecular interactions in the crystal structure of **4** reveals that the interaction mediated by O3–H3···O17^{i} hydrogen bond is one of the four most dominant. Its energy amounts to −37 kJ mol^{-1}, and it is the only one in which the electrostatic and dispersion terms contribute equally to its stabilizing character. This is a consequence of the good complementarity in electrostatic potentials mapped on Hirshfeld surfaces of the adjoining molecules in the vicinity of hydrogen bonding interacting atoms, as well as the fact that matching

TABLE 4 Summary of intermolecular interaction energies of the unique molecular pairs constituting the first coordination sphere for **3** and **4** calculated using the CE-B3LYP energy model

				E/kJ mol^{-1}				
Label	***N***	**Symmetry operation**	***R*/Å**	E_{ele}	E_{pol}	E_{dis}	E_{rep}	E_{tot}
3								
1	2	x, y, z	6.79	−25.5	−5.3	−106.3	77.0	−75.9
2	2	x, y, z	18.25	−3.3	−0.6	−16.1	10.0	−11.8
3	2	$-x, y + ½, -z + ½$	9.81	−1.7	−0.2	−11.6	2.7	−10.4
4	2	$x + ½, -y + ½, -z$	12.37	−5.1	−0.5	−21.7	15.1	−15.3
5	2	x, y, z	13.96	−3.8	−0.7	−26.0	17.3	−16.6
6	2	$x + ½, -y + ½, -z$	7.87	−3.0	−1.5	−18.8	6.0	−17.0
7	2	$-x, y + ½, -z + ½$	9.86	−10.1	−3.9	−27.0	19.8	−24.9
8	2	$x + ½, -y + ½, -z$	12.42	−3.7	−0.5	−15.4	10.3	−11.3
9	2	$-x, y + ½, -z + ½$	13.79	−3.0	−1.9	−15.6	5.0	−15.1
4								
1	2	$-x, y + ½, -z + ½$	9.20	−11.5	−3.3	−53.7	26.6	−44.9
2	2	$x + ½, -y + ½, -z$	6.96	−10.6	−2.1	−63.2	36.0	−45.6
3	2	x, y, z	7.44	−8.5	−3.2	−51.0	29.7	−37.4
4	2	x, y, z	13.11	−30.4	−5.6	−27.2	36.6	−37.4
5	2	$-x, y + ½, -z + ½$	12.57	−3.8	−2.0	−14.4	8.2	−12.9
6	2	x, y, z	15.07	−5.0	−2.1	−17.0	12.0	−14.3
7	1	$x + ½, -y + ½, -z$	16.32	−0.3	−0.1	−1.8	0.0	−1.9
8	2	$x + ½, -y + ½, -z$	12.62	−0.4	−0.0	−2.0	0.0	−2.2

Note. N is the number of interactions; R is the distance between molecular centroids. The relevant space group symmetry operation is reported without translation. $E_{tot} = k_{ele}E_{ele} + k_{pol}E_{pol} + k_{dis}E_{dis} + k_{rep}E_{rep}$, where $k_{ele} = 1.057$, $k_{pol} = 0.740$, $k_{dis} = 0.871$, and $k_{rep} = 0.618$.[36]

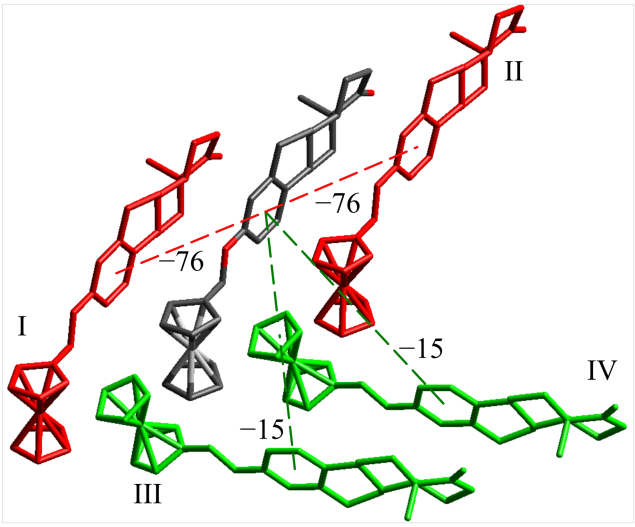

FIGURE 7 Two types of ferrocene–ferrocene dimers in the crystal structure of **3**. Dashed lines connecting centroids of the molecules are labeled with calculated interaction energies in kilojoule per mol^{e}. Symmetry operations employed to generate molecules: $x + 1, y, z$ for I; $x - 1, y, z$ for II; $x + ½, -y + ½, -z + 1$ for III, $x - ½, -y + ½, -z + 1$ for IV

patches of the Hirshfeld surfaces accumulate the highest absolute values of the electrostatic potential present on the Hirshfeld surfaces, as visualized in Figure S17. The other three interactions are dispersion-dominated and comparably strong (−37 to −46 kJ mol^{-1}), and in addition to these, there are four considerably weaker interactions (−2 to −14 kJ mol^{-1}). Therefore, no single motif can be selected as the basic structural unit of the crystal structure of **4**, and it can be seen from the corresponding energy framework (Figure 6c,d) that interactions are isotropically distributed in the crystal structure. Intermolecular interactions between the central molecule and neighbors comprising the first coordination shell, present in the crystal structure of **4**, are summarized in Table 4.

3.4 | Electrochemistry

As our current understanding of the cytotoxicity of ferrocene compounds bases itself on the hypothesis that ultimately oxidation to ferrocenium must occur in biological systems, we found it important to investigate the redox

properties of the newly synthesized ferrocene–steroid conjugates. The parent steroids (E2 and E1) and the ferrocene–steroid conjugates **1**–**5** were electrochemically studied in DMF at a GC electrode. As previously mentioned, pure samples of compounds **4** and **5** were unavailable; the 7:3 mixture of **4** and **5** was studied. The available potential range was −2.0 to +1.5 V; the applied scan rates varied from 0.01 to 5 V s^{-1}.

To understand the electrochemical properties of the conjugates more completely, it was necessary to first investigate the redox properties of E2 and E1 under the same experimental conditions. The electrochemical behavior of E2, E1, and other phenols was previously a subject of a number of studies.[50] It was shown that the oxidation process involving this group might proceed through the release of usually $2e^-$ in total accompanied by chemical steps, mainly following two reaction pathways and involving the reversible formation of either phenoxide radical, and eventually, irreversibly, their dimers, or quinoidal structures. All the processes were greatly dependent on the nature of the solvent, pH, and, to some extent, the working electrode.[50]

The oxidation of E2 and E1, which displayed similar voltammograms, occurred in one irreversible peak (E, Figure 8) at potentials of about +1.1 V. The current function $I_p/cv^{1/2}$ was about two times larger than that of the molecule of ferrocene alone. Other parameters were: $\Delta E_p/\Delta \log v \sim 40$ mV dec^{-1} at $v < 100$ mV s^{-1} reaching 70 mV dec^{-1} at $v \sim 1$ V s^{-1}; half-peak width varied from ∼ 65 mV at $v = 20$ mV s^{-1} to ∼ 130 mV at 500 mV s^{-1}. These characteristics correspond to an irreversible oxidation process composed of two closed 1-e^- steps coupled to a chemical reaction. The product of this reaction, reducible at ∼ −0.3 V, was not identified. The repetitive cycling of the potential in the range from −0.6 to +1.5 V led to a 10%–20% current decrease of the main peak at higher scan rates, which was not observed at the lower ones. This suggests that the reactant at −0.3 V is only an intermediate that can be converted to the starting compound. This might be a phenoxide radical (dimer), as suggested in some studies[50] at different experimental conditions. However, for an explicit conclusion, more experiments are needed.

Compounds **1**–**5** have a pair of peaks located at about +0.5 V corresponding to redox processes at the ferrocenyl moiety (peaks F/F′). The other oxidation peak E at potentials of about +1.1 V appears in voltammograms of **2** and the mixture of **4** and **5** and belongs to the process described earlier. In contrast to that, cyclic voltammograms of **1** and **3** lack this peak due to the absence of the phenol group. To illustrate this, typical cyclic voltammograms of **1** and **2** are shown in Figure 9. The voltammograms of the mixture of **4** and **5** appeared similar to those of compound **2** (Figure S18), suggesting that there are no drastic differences in the electrochemical properties of the ferrocenyl cores among the regioisomers. Peak potentials and their current functions for all of these compounds are given in Table 5. An interesting difference can be observed regarding the peak currents for the E peaks in E1 and E2, and their ferrocene conjugates **2**, **4,** and **5**. In the latter compounds, the peak current ratio of ferrocenyl and phenolic moieties is about 1:3. Obviously, the current functions are higher for the conjugates than for E2 and E1 alone. Although the

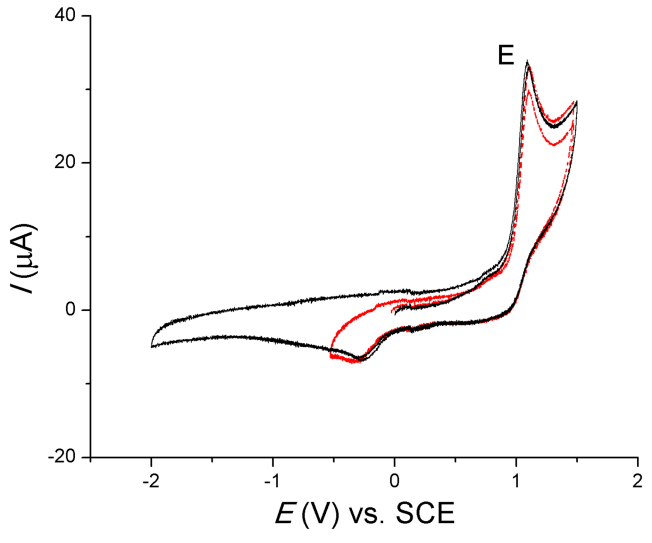

FIGURE 8 Cyclic voltammograms for E2 (1.2 mM) in DMF + 0.1 M TBAP at two different potential ranges (— and - - -); GC electrode, $v = 0.10$ V s^{-1}

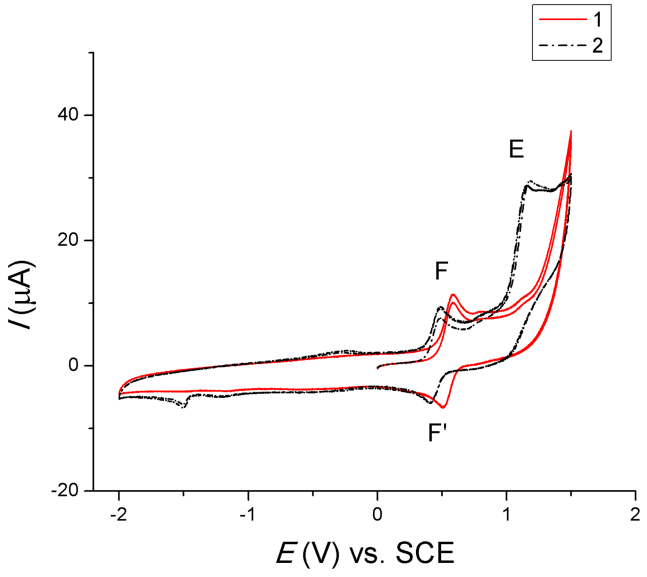

FIGURE 9 Cyclic voltammograms for **1** (0.65 mM) and **2** (0.52 mM) in DMF + 0.1 M TBAP; GC electrode, $v = 0.10$ V s^{-1}

TABLE 5 Cyclic voltammetric peak potentials and current functions for E1, E2, and **1–5**; GC electrode, $v = 0.10$ V/s

Compound	E_p^{Fa}	$I_p/cv^{1/2b}$	E_p^{E}	$I_p/cv^{1/2}$
E1	–	–	1.15	87.1
E2	–	–	1.18	84.2
1	0.59	43.1	–	–
2	0.49	40.3	1.18	120.4
3	0.59	44.6	–	–
4 + 5	0.47	38.4	1.17	106.0

[a]In V vs. SCE.
[b]In μA/mM(V/s)$^{1/2}$.

TABLE 6 Electrochemical data of ferrocene peak potentials and apparent heterogeneous rate constant

Compound	E_p^{aa}	E_p^{c}	$E^{0'}$	ΔE_p^{b}	$k^{0'} \times 10^{4c}$
Fc	0.532	0.447	0.490	85	1.0 ± 0.2
1	0.589	0.515	0.552	74	1.3 ± 0.1
2	0.486	0.414	0.450	72	1.4 ± 0.3
3	0.588	0.516	0.552	72	1.4 ± 0.3
4 + 5	0.470	0.398	0.434	72	1.4 ± 0.3

[a]In V vs. SCE.
[b]In mV.
[c]In ms^{-1}.

general appearance and potentials of these peaks are similar to those of the parent compounds, the currents suggest a different reaction mechanism leading to a presumption of a one-step 2-e$^-$ transfer. A more detailed study must be done to achieve a thorough insight into the processes that are out of the scope of the present work.

To elucidate how the conjugation with E2 and E1 affects the redox process at the ferrocene moiety, we limited the potential scan only to the first oxidation process. This is illustrated in Figure 10 where the effects of the two modes of ferrocene attachment to the steroid core in **1** and **2** are compared to the behavior of ferrocene itself. The characteristics of these processes are given in Table 6. In comparison to ferrocene, compounds **2**, **4**, and **5** have about 40–55 mV less anodic peaks, while **1** and **3** have about 60 mV more anodic peaks. Interestingly, not only are the potentials affected, but also the

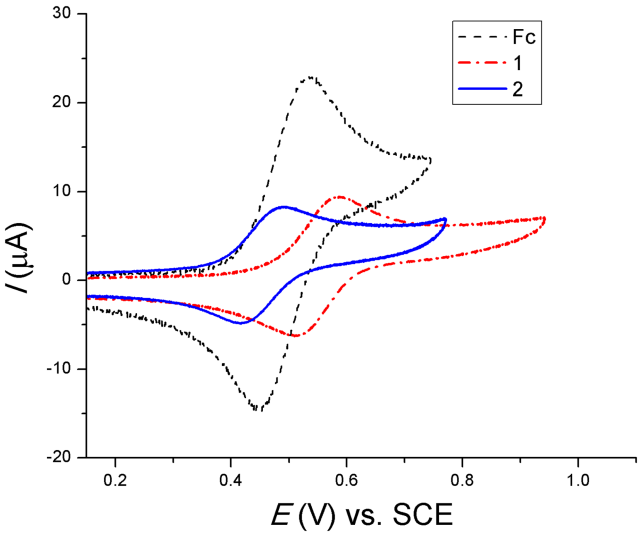

FIGURE 10 Cyclic voltammograms of ferrocene (Fc, 1.0 mM) and the ferrocenyl moiety of **1** (0.65 mM) and **2** (0.52 mM) in DMF + 0.1 M TBAP; GC electrode, $v = 0.10$ V/s

reversibility is improved in all of these cases (judging from the $\Delta E_p^{a/c}$ for ferrocene and the conjugates). We found it interesting to illustrate this effect by calculating the heterogeneous rate constants for ferrocene and compounds **1–5** using the well-known Nicholson equation for quasireversible processes.[51] To calculate this, we applied a diffusion coefficient D value for ferrocene in DMF of 9.5×10^{-10} m^2 s^{-1}.[52] For these calculations, we did not determine D values for our compounds experimentally but used their estimated values from a comparison of the current functions of oxidation peaks for each compound and ferrocene alone, recorded under the same voltammetric conditions. It appeared that the ratio of these currents was ~40:60 μA mM^{-1} V$^{-1/2}$ s$^{1/2}$, which led us to conclude that D coefficients are lower for the conjugates, and are ~ 4.2×10^{-10} m^2 s^{-1}. Finally, for the scan rates of 20– 200 mV s^{-1}, the calculated values of $k^{0'}$ are given in Table 6. It appears that the oxidation process of ferrocene in compounds **1–5** is more reversible than that of ferrocene itself. In addition, all of the values lay at the lower limit for quasireversible processes,[53] which is a very favorable feature, especially for the fact that no *IR* compensation was carried out in these measurements.

3.5 | Antiproliferative activity

The synthesized compounds were tested against a panel of cancer cell lines that included estrogen receptor-positive breast adenocarcinoma MCF-7, estrogen receptor-negative breast adenocarcinoma MDA-MB-231, prostate cancer PC-3, cervical carcinoma HeLa, colon adenocarcinoma HT-29, and lung adenocarcinoma A549. In addition, normal fetal lung fibroblasts MRC-5 were used as a human noncancerous cell line. As in the electrochemistry experiments, the 7:3 mixture of compounds **4** and **5** was used for the antiproliferative activity assays. The *in vitro* antiproliferative activity was determined after a 72-h cell

TABLE 7 Antiproliferative activity of compounds **1**–**5** and doxorubicin (DOX) expressed as $IC_{50} \pm SD$

	IC_{50} (μM)						
Compound(s)	**MCF-7**	**MDA-MB-231**	**PC-3**	**HeLa**	**HT-29**	**A549**	**MRC-5**
1	20 ± 4	49 ± 7	> 100	> 100	> 100	> 100	> 100
2	0.34 ± 0.05	> 100	> 100	> 100	> 100	84 ± 22	> 100
3	> 100	60 ± 4	> 100	> 100	> 100	> 100	> 100
4 + **5**	> 100	64 ± 9	27 ± 9	> 100	> 100	> 100	> 100
DOX	0.69 ± 0.09	0.15 ± 0.04	94 ± 12	1.52 ± 0.17	0.14 ± 0.05	8 ± 2	0.15 ± 0.07

treatment by the MTT assay. The chemotherapeutic DOX was used as a positive control.

The results of the experiments are presented in Table 7. All of the ferrocene–steroid conjugates did not exhibit cytotoxicity against MRC-5 cells. Except in two cases, these compounds showed no significant antiproliferative activity against PC-3, HeLa, HT-29, and A549, with their IC_{50} values being greater than 100 μM. One exception was the antiproliferative activity of **4** and **5** toward PC-3 (IC_{50} = 27 μM), and the other was the activity of **2** toward A549 (84 μM).

As expected, MCF-7 and MDA-MB-231 were most sensitive to the ferrocene-estrogen conjugates. Compound **2** with its submicromolar IC_{50} value of 0.34 μM for MCF-7 showed the strongest antiproliferative effect. Against this cell line, it was even somewhat more potent than DOX; to the best of our knowledge, this result makes compound **2** the most cytotoxic ferrocene–steroid conjugate reported to date. Compound **1** also displayed a notable effect on MCF-7 (20 μM), while MDA-MB-231 cells were moderately affected (∼50–60 μM, statistically insignificant differences in the activity) by all compounds except compound **2**.

Unlike the previously reported 7α- and 17α-derivatives, not one of these compounds was found to possess a proliferative effect on MCF-7, suggesting that, in all probability, functionalizing the steroid A ring with a bulky ferrocene residue rids the molecule of most of its estrogenicity, allowing the intrinsic cytotoxicity of ferrocene to be manifested. This is consistent with the hypothesis set out by Jaouen and coworkers[54] that the antiproliferative activity of steroidal androgen–ferrocene conjugates is influenced both by the proliferation-inducing androgenicity of the molecule and by the cytotoxic properties caused by ferrocene. However, as some compounds were significantly more active against MCF-7 than others, it remains reasonable to attribute a portion of the activity to the steroid core and substitution mode. In other words, estrone derivatives possessed only a weak activity, while estradiol derivatives showed a medium or very strong response, depending on whether it was the product of 3-*O*- (**1**) or 4-*C*-alkylation (**2**), respectively. Despite the observation that 4-*C*-alkylation results in conjugates that are more easily oxidized compared to the products of 3-*O*-alkylation, no definitive conclusions about the influence of the redox potential on the antiproliferative activity could be drawn from the results of this work.

4 | CONCLUSIONS

Five new ferrocene–estra-1,3,5(10)-triene conjugates (**1**–**5**) were synthesized by ferrocenylmethylation of E2 and E1. All of the conjugates were fully spectrally characterized (NMR, IR, UV–Vis., HRMS), while single-crystal X-ray diffraction analysis was performed on conjugates **3** and **4**. The redox properties of the conjugates were investigated by cyclic voltammetry. The conjugates were screened for *in vitro* antiproliferative activity against six human cancerous cell lines. While a wide range of activities were observed, the activity of compound **2** on the hormone-dependent breast cancer cells stood out; its IC_{50} value of 0.34 μM was lower than that of DOX, or for that matter, any other previously reported value for a ferrocene–steroid conjugate. None of the compounds were toxic to fetal human fibroblasts, a noncancerous cell line. These results point to A-ring substitution of steroidal estrogens as a plausible strategy for preparing other ferrocene–steroid conjugates acting against tumor cells.

ACKNOWLEDGMENTS

This work was supported by the Ministry of Education, Science and Technological Development of the Republic of Serbia (Grant No. 451-03-68/2020-14/200125). NR is grateful to the same Ministry for financial support (Project No. 172061, Grant No. 451-03-68/2020-14/200124). MR is grateful to the Deutscher Akademischer Austauschdienst (DAAD) for the awarded scholarship in

the Research Stays for University Academics and Scientists programme in 2018.

ORCID

Vidak Raičević https://orcid.org/0000-0002-3858-4350
Niko Radulović https://orcid.org/0000-0003-1342-7567
Ljiljana Jovanović https://orcid.org/0000-0001-8773-774X
Marko Rodić https://orcid.org/0000-0002-4471-8001
Ivana Kuzminac https://orcid.org/0000-0001-8045-3568
Dimitar Jakimov https://orcid.org/0000-0002-1747-4718
Tanja Wrodnigg https://orcid.org/0000-0002-7644-5431
Tim-Oliver Knedel https://orcid.org/0000-0002-2072-3332
Christoph Janiak https://orcid.org/0000-0002-6288-9605
Marija Sakač https://orcid.org/0000-0002-2796-1296

REFERENCES

[1] B. W. Stewart, C. P. Wild (Eds), *World Cancer Report 2014*, Lyon, France **2014**.
[2] (a) S. Masood, *Diagn. Cytopathol.* **1992**, *8*, 475. (b) W. F. Anderson, N. Chatterjee, W. B. Ershler, O. W. Brawley, *Breast Cancer Res. Treat.* **2002**, *76*, 27. (c) N. Bentzon, M. Düring, B. B. Rasmussen, H. Mouridsen, N. Kroman, *Int. J. Cancer* **2008**, *122*, 1089.
[3] (a) S. Nilsson, S. Mäkelä, E. Treuter, M. Tujague, J. Thomsen, G. Andersson, E. Enmark, K. Pettersson, M. Warner, J.-Å. Gustafsson, *Physiol. Rev.* **2001**, *81*, 1535. (b) C. Williams, C.-Y. Lin, *Ecancermedicalscience* **2013**, *7*, 370. (c) P. Yaşar, G. Ayaz, S. D. User, G. Güpür, M. Muyan, *Reprod. Med. Biol.* **2016**, *16*, 4. (d) K. S. Korach, S. C. Hewitt, K. J. Hamilton, Y. Li, J. T. Ramsey, M. Garcia, E. Mathura, Y. Arao, in *Estrogen Receptor and Breast Cancer*, (Ed: X. Zhang), Springer International Publishing, Cham **2019**.
[4] W. J. Gradishar, *Oncol.* **2004**, *9*, 378.
[5] C. Furman, M.-H. Hao, S. Prajapati, D. Reynolds, V. Rimkunas, G. Z. Zheng, P. Zhu, M. Korpal, *Cancer Res.* **2019**, *79*, 1740.
[6] (a) R. S. Braithwaite, R. T. Chlebowski, J. Lau, S. George, R. Hess, N. F. Col, *J. Gen. Intern. Med.* **2003**, *18*, 937. (b) C. D. Bushnell, L. B. Goldstein, *Neurology* **2004**, *63*, 1230. (c) V. C. Jordan, B. W. O'Malley, *J. Clin. Oncol.* **2007**, *25*, 5815. (d) J. E. Garber, S. Halabi, S. M. Tolaney, E. Kaplan, L. Archer, J. N. Atkins, S. Edge, C. L. Shapiro, L. Dressler, E. D. Paskett, G. Kimmick, J. Orcutt, A. Scalzo, E. Winer, E. Levine, N. Shahab, Cancer and Leukemia Group B, *J. Natl. Cancer Inst.* **2010**, *102*, 942.
[7] (a) I. A. Shagufta, *Eur. J. Med. Chem.* **2018**, *143*, 515. (b) J. Liu, B. Ming, G.-H. Gong, D. Wang, G.-L. Bao, L.-J. Yu, *RSC Adv.* **2018**, *8*, 4386.
[8] H. Werner, *Angew. Chemie Int. Ed.* **2012**, *51*, 6052.
[9] (a) P. Köpf-Maier, H. Köpf, E. W. Neuse, *Angew. Chemie Int. Ed. English* **1984**, *23*, 456. (b) P. Köpf-Maier, H. Köpf, E. W. Neuse, J. Cancer, *Res. Clin. Oncol.* **1984**, *108*, 336.
[10] (a) D. Osella, M. Ferrali, P. Zanello, F. Laschi, M. Fontani, C. Nervi, G. Cavigiolio, *Inorganica Chim. Acta* **2000**, *306*, 42. (b) G. Tabbì, C. Cassino, G. Cavigiolio, D. Colangelo, A. Ghiglia, I. Viano, D. Osella, *J. Med. Chem.* **2002**, *45*, 5786.
[11] E. W. Neuse, M. G. Meirim, N. F. Blom, *Organometallics* **1988**, *7*, 2562.
[12] E. W. Neuse, F. Kanzawa, *Appl. Organomet. Chem.* **1990**, *4*, 19.
[13] C.-W. Ong, J.-Y. Jeng, S.-S. Juang, C.-F. Chen, *Bioorg. Med. Chem. Lett.* **1992**, *2*, 929.
[14] N. Metzler-Nolte, M. Salmain, in *Ferrocenes: Ligands, Materials and Biomolecules*, (Ed: P. Štěpnička), John Wiley & Sons, Chichester, England **2008**.
[15] (a) C. Ornelas, *New J. Chem.* **2011**, *35*, 1973. (b) F. A. Larik, A. Saeed, T. A. Fattah, U. Muqadar, P. A. Channar, *Appl. Organomet. Chem.* **2017**, *31*, e3664. (c) M. Patra, G. Gasser, *Nat. Rev. Chem.* **2017**, *1*, 66.
[16] E. A. Hillard, A. Vessières, G. Jaouen, in *Medicinal Organometallic Chemistry*, (Eds: G. Jaouen, N. Metzler-Nolte), Springer, Berlin **2010**.
[17] (a) A. Vessières, C. Vaillant, M. Gruselle, D. Vichard, G. Jaouen, *J. Chem. Soc., Chem. Commun.* **1990**, 837. (b) D. Vichard, M. Gruselle, G. Jaouen, M. N. Nefedova, I. A. Mamedyarova, V. I. Sokolov, J. Vaissermann, *J. Organomet. Chem.* **1994**, *484*, 1. (c) D. Osella, C. Nervi, F. Galeotti, G. Cavigiolio, A. Vessières, G. Jaouen, *Helv. Chim. Acta* **2001**, *84*, 3289. (d) A. Vessières, D. Spera, S. Top, B. Misterkiewicz, J.-M. Heldt, E. Hillard, M. Huché, M.-A. Plamont, E. Napolitano, R. Fiaschi, G. Jaouen, *ChemMedChem* **2006**, *1*, 1275.
[18] (a) M. Wenzel, *J. Labelled Compd. Radiopharm.* **1992**, *31*, 641. (b) M. Wenzel, C. Klinge, *J. Labelled Compd. Radiopharm.* **1994**, *34*, 981.
[19] J. Manosroi, K. Rueanto, K. Boonpisuttinant, W. Manosroi, C. Biot, H. Akazawa, T. Akihisa, W. Issarangporn, A. Manosroi, *J. Med. Chem.* **2010**, *53*, 3937.
[20] J. A. Carmona-Negrón, A. Santana, A. L. Rheingold, E. Meléndez, *Dalt. Trans.* **2019**, *48*, 5952.
[21] E. Palomino, *Crit. Rev. Biochem. Mol. Biol.* **1999**, *34*, 387.
[22] K. Wang, S. Muñoz, L. Zhang, R. Castro, A. E. Kaifer, G. W. Gokel, *J. Am. Chem. Soc.* **1996**, *118*, 6707.
[23] K. Hoffmann, B. Rießelmann, M. Wenzel, *Liebigs Ann. der Chemie* **1980**, *1980*, 1181.
[24] J. Vera, L. M. Gao, A. Santana, J. Matta, E. Meléndez, *Dalt. Trans.* **2011**, *40*, 9557.
[25] (a) J. J. Ajduković, K. M. Penov Gaši, D. S. Jakimov, O. R. Klisurić, S. S. Jovanović-Šanta, M. N. Sakač, L. D. Aleksić, E. A. Djurendić, *Bioorg. Med. Chem.* **2015**, *23*, 1557. (b) S. Bjedov, D. Jakimov, M. Poša, O. R. Klisurić, M. Sakač, *Tetrahedron* **2017**, *73*, 6932. (c) A. R. Nikolić, I. Z. Kuzminac, S. S. Jovanović-Šanta, D. S. Jakimov, L. D. Aleksić, M. N. Sakač, *Steroids* **2018**, *135*, 101. (d) N. S. Radulović, D. B. Zlatković, K. V. Mitić, P. J. Randjelović, N. M. Stojanović, *Polyhedron* **2014**, *80*, 134. (e) A. Pejović, M. S. Denić, D. Stevanović, I. Damljanović, M. Vukićević, K. Kostova, M. Tavlinova-Kirilova, P. Randjelović, N. M. Stojanović, G. A. Bogdanović, P. Blagojević, M. D'hooghe, N. S. Radulović, R. D. Vukićević, *Eur. J. Med. Chem.* **2014**, *83*, 57. (f) N. S. Radulović, M. Z. Mladenović, Z. Stojanović-Radić, G. A. Bogdanović, D. Stevanović, R. D. Vukićević, *Mol. Diversity* **2014**, *18*, 497.
[26] D. Lednicer, C. R. Hauser, *Org. Synth.* **1960**, *40*, 31.

[27] V. Nagy, A. Agócs, E. Turcsi, J. Deli, *Phytochem. Anal.* **2009**, *20*, 143.
[28] G. M. Sheldrick, *Acta Crystallogr. Sect. A* **2015**, *71*, 3.
[29] G. M. Sheldrick, *Acta Crystallogr. Sect. C* **2015**, *71*, 3.
[30] C. B. Hübschle, G. M. Sheldrick, B. Dittrich, *J. Appl. Crystallogr.* **2011**, *44*, 1281.
[31] J. Luebben, T. Gruene, *Proc. Natl. Acad. Sci.* **2015**. https://doi.org/10.1073/pnas.1502136112
[32] A. L. Spek, *Acta Crystallogr. Sect. D* **2009**, *65*, 148.
[33] C. F. Macrae, I. J. Bruno, J. A. Chisholm, P. R. Edgington, P. McCabe, E. Pidcock, L. Rodriguez-Monge, R. Taylor, J. van de Streek, P. A. Wood, *J. Appl. Crystallogr.* **2008**, *41*, 466.
[34] (a) M. A. Spackman, P. G. Byrom, *Chem. Phys. Lett.* **1997**, *267*, 215. (b) M. A. Spackman, J. J. McKinnon, *CrystEngComm* **2002**, *4*, 378.
[35] M. J. Turner, J. J. McKinnon, S. K. Wolff, D. J. Grimwood, P. R. Spackman, D. Jayatilaka, M. A. Spackman, **2017**.
[36] C. F. Mackenzie, P. R. Spackman, D. Jayatilaka, M. A. Spackman, *IUCrJ* **2017**, *4*, 575.
[37] M. J. Turner, S. P. Thomas, M. W. Shi, D. Jayatilaka, M. A. Spackman, *Chem. Commun.* **2015**, *51*, 3735.
[38] J. Juillard, in *Recommended Methods for Purification of Solvents and Tests for Impurities*, (Ed: J. F. Coetzee), Pergamon, Oxford **1982**.
[39] (a) A. A. van de Loosdrecht, R. H. J. Beelen, G. J. Ossenkoppele, M. G. Broekhoven, M. M. A. C. Langenhuijsen, *J. Immunol. Methods* **1994**, *174*, 311. (b) N. Stojiljković, S. Ilić, N. Stojanović, S. Stojanović, M. Stoiljković, *Can. J. Physiol. Pharmacol.* **2019**. https://doi.org/10.1139/cjpp-2019-0251
[40] (a) D. E. Bublitz, K. L. Rinehart Jr., *Org. React.* **2011**, 1. (b) V. I. Boev, L. V. Snegur, V. N. Babin, Y. S. Nekrasov, *Russ. Chem. Rev.* **1997**, *66*, 613.
[41] A. N. Nesmeyanov, E. G. Perevalova, L. S. Shilovtseva, Y. A. Ustynyuk, *Dokl. Akad. Nauk SSSR* **1959**, *124*, 331.
[42] Y. Yamaguchi, W. Ding, C. T. Sanderson, M. L. Borden, M. J. Morgan, C. Kutal, *Coord. Chem. Rev.* **2007**, *251*, 515.
[43] (a) P. Ciuffreda, P. Ferraboschi, E. Verza, A. Manzocchi, *Magn. Reson. Chem.* **2001**, *39*, 648. (b) J. Guo, R. I. Duclos Jr., V. K. Vemuri, A. Makriyannis, *Tetrahedron Lett.* **2010**, *51*, 3465.
[44] I. J. Bruno, J. C. Cole, M. Kessler, J. Luo, W. D. S. Motherwell, L. H. Purkis, B. R. Smith, R. Taylor, R. I. Cooper, A. G. Orpen, *J. Chem. Inf. Comput. Sci.* **2004**, *44*, 2133.
[45] (a) D. Cremer, J. A. Pople, *J. Am. Chem. Soc.* **1975**, *97*, 1354. (b) D. G. Evans, J. C. A. Boeyens, *Acta Crystallogr. Sect. B* **1989**, *45*, 581.
[46] J. C. A. Boeyens, *J. Cryst. Mol. Struct.* **1978**, *8*, 317.
[47] C. Jelsch, K. Ejsmont, L. Huder, *IUCrJ* **2014**, *1*, 119.
[48] (a) A. Gavezzotti, *CrystEngComm* **2013**, *15*, 4027. (b) A. J. Edwards, C. F. Mackenzie, P. R. Spackman, D. Jayatilaka, M. A. Spackman, *Faraday Discuss.* **2017**, *203*, 93.
[49] G. A. Bogdanović, S. B. Novaković, *CrystEngComm* **2011**, *13*, 6930.
[50] (a) L. Papouchado, R. W. Sandford, G. Petrie, R. N. Adams, *J. Electroanal. Chem. Interfacial Electrochem.* **1975**, *65*, 275. (b) M. M. Ngundi, O. A. Sadik, T. Yamaguchi, S. Suye, *Electrochem. Commun.* **2003**, *5*, 61. (c) P. Gan, R. G. Compton, J. S. Foord, *Electroanalysis* **2013**, *25*, 2423.
[51] R. S. Nicholson, *Anal. Chem.* **1965**, *37*, 1351.
[52] N. G. Tsierkezos, *J. Solution Chem.* **2007**, *36*, 289.
[53] P. Zanello, *Inorganic Electrochemistry: Theory*, Practice and Applications, The Royal Society Of Chemistry, Cambridge **2003**.
[54] S. Top, C. Thibaudeau, A. Vessières, E. Brulé, F. Le Bideau, J.-M. Joerger, M.-A. Plamont, S. Samreth, A. Edgar, J. Marrot, P. Herson, G. Jaouen, et al., *Organometallics* **2009**, *28*, 1414.

SUPPORTING INFORMATION

Additional supporting information may be found online in the Supporting Information section at the end of this article.

How to cite this article: Raičević V, Radulović N, Jovanović L, et al. Ferrocenylmethylation of estrone and estradiol: Structure, electrochemistry, and antiproliferative activity of new ferrocene–steroid conjugates. *Appl Organomet Chem*. 2020;34: e5889. https://doi.org/10.1002/aoc.5889